Magnetic Resonance Imaging 60 (2019) 44–51

Contents lists available at ScienceDirect

Magnetic Resonance Imaging

journal homepage: www.elsevier.com/locate/mri

Original contribution

Clinical feasibility of brain quantitative susceptibility mapping

Shun Zhang[a,b], Zhe Liu[a,c], Thanh D. Nguyen[a], Yihao Yao[b], Kelly M. Gillen[a], Pascal Spincemaille[a], Ilhami Kovanlikaya[a], Ajay Gupta[a], Yi Wang[a,c,*]

[a] Department of Radiology, Weill Cornell Medicine, New York, NY, USA
[b] Department of Radiology, Tongji Hospital, Tongji Medical College, Huazhong University of Science and Technology, Wuhan, China
[c] Department of Biomedical Engineering, Cornell University, Ithaca, NY, USA

ARTICLE INFO

Keywords:
Quantitative susceptibility mapping
Zero reference
Cerebrospinal fluid
Morphology enabled dipole inversion
Multiple sclerosis

ABSTRACT

Purpose: To evaluate the quality of brain quantitative susceptibility mapping (QSM) that is fully automatically reconstructed in clinical MRI of various neurological diseases.

Methods: 393 consecutive patients in one month were recruited for this evaluation study. QSM was reconstructed using Morphology Enabled Dipole Inversion without zero reference regularization (MEDI) and using MEDI with cerebrospinal fluid automatic zero-reference regularization to generate susceptibility values (MEDI + 0). Two neuroradiologists independently assessed the image quality of MEDI + 0 and MEDI and image concordance between them. Lesion susceptibility values were measured in 20 cases of glioma, 21 cases of ischemic stroke and 43 multiple sclerosis (MS) cases on both MEDI + 0 and MEDI images.

Results: The two neuroradiologists rated the MEDI + 0 image qualities of the 393 cases as 351 (89.3%) and 362 (92.1%) excellent, 29 (7.4%) and 24 (6.1%) diagnostic, and 13 (3.3%) and 7 (1.8%) poor, and scored the concordances between MEDI + 0 and MEDI as 364 (92.6%) and 351 (89.3%) excellent, 13 (3.3%) and 31 (7.9%) good, 14 (3.6%) and 9 (2.3%) intermediate, 2 (0.5%) and 2 (0.5%) poor, and 0 (0%) and 0 (0%) none. There was good correlation between MEDI + 0 and MEDI in lesion susceptibility contrast of glioma, ischemic stroke, and MS cases (all $p < 0.05$). The MS lesion susceptibility time course from this patient cohort was found to be similar to the reported pattern: isointense initially for acute enhancing lesions, and hyperintense over the following years for active chronic lesions.

Conclusion: Brain QSM images of various neurological diseases have reliable diagnostic quality in clinical MRI, with MEDI + 0 providing susceptibility values automatically referenced to CSF in longitudinal and cross-center studies.

1. Introduction

Quantitative susceptibility mapping (QSM) overcomes blooming artifacts in susceptibility based magnitude and phase images [1] by identifying the field generated by tissue magnetic susceptibility [2] and solving the field to susceptibility source inverse problem using prior knowledge in the optimal Bayesian inference [3]. QSM has been used increasingly in studying diseases involving magnetic susceptibility changes in brain tissues [4–8], including multiple sclerosis (MS) [9–18], Parkinson's disease [19–22], calcifications, hemorrhage [23–27], and gliomas [28].

Conventional QSM reconstructions [5–8], such as Morphology Enabled Dipole Inversion (MEDI) [29–31], use structural prior information only and require a reference region of interest (ROI) to provide susceptibility value. For longitudinal and cross-center studies, an ROI drawn in cerebrospinal fluid (CSF) or normal appearing white matter (NAWM) is usually selected as a reference [10–12, 32]. However, the susceptibility of ventricular CSF is inhomogeneous as a result of the anisotropy of the surrounding white matter tracts [33,34]; and NAWM may be involved in disease, and its appearance is orientation-dependent on white matter tracts [34–40]. These factors may cause bias in selecting NAWM or CSF as a reference for conventional QSM.

MEDI reconstructed with an additional zero-susceptibility regularization on the ventricular CSF (MEDI + 0) solves this tissue reference problem. MEDI + 0 reconstruction improves QSM image quality, providing a realistic uniform CSF and reducing shadow artifacts [41]. MEDI + 0 can be performed on the same gradient echo data as that input into MEDI.

For technique dissemination and clinical translation, we have made the full codes of MEDI + 0 and MEDI freely downloadable at med.

* Corresponding author at: Radiology, Weill Cornell Medicine, 515 E 71st Street, Suite 102, New York, NY 10021, USA.
E-mail address: yiwang@med.cornell.edu (Y. Wang).

https://doi.org/10.1016/j.mri.2019.04.003
Received 7 January 2019; Received in revised form 31 March 2019; Accepted 2 April 2019

cornell.edu/mri. In conjunction with the code engineering efforts, we report here QSM performance, including both MEDI + 0 and MEDI, in various neurological diseases in a clinical setting.

2. Materials and methods

This study was approved by our local Institutional Review Board, written informed consent was waived for this retrospective analysis.

2.1. Patient selection and data acquisitions

A total of 393 consecutive cases with brain 3D multi echo gradient echo (GRE) scans in one month from three clinical scanners at our institution were included in this study and used for qualitative analysis: GE Signa HDxt 3.0 T (field of view = 24 cm, TR = 69 ms, TE1/ΔTE = 4.6/4.8 ms, number of TEs = 11, acquisition matrix = 416 × 320, readout bandwidth = 244 Hz/pixel, slice thickness = 3 mm, flip angle = 20); GE Discovery 750w 3.0 T (field of view = 24 cm, TR = 66 ms, TE1/ΔTE = 4.8/10.5 ms, number of TEs = 6, acquisition matrix = 416 × 256, readout bandwidth = 244 Hz/pixel, slice thickness = 3 mm, flip angle = 20°); Siemens Skyra 3.0 T (field of view = 24 cm, TR = 49 ms, TE1/ΔTE = 6.7/4.1 ms, number of TEs = 10, acquisition matrix = 320 × 190, readout bandwidth = 260 Hz/pixel, slice thickness = 3 mm, flip angle = 15°). This cohort includes 27 cases of multiple sclerosis (MS) that are part of a longitudinal, prospective MS MRI and clinical database, which were also selected for susceptibility time course analysis. In addition to 3D GRE, the MS MRI protocol included the following standard clinical imaging sequences: 3D T1 weighted (T1w), 2D T2 weighted (T2w), 3D T2w FLAIR, and post-gadolinium (Gd) 3D T1w (T1w + Gd).

In addition, in order to compare MEDI and MEDI + 0 quantitatively, another dataset consisting of 20 cases of brain glioma, 21 cases of ischemic stroke, and 43 cases of MS were also consecutively collected for evaluation of lesion susceptibility measurements: GE Discovery 750 3.0 T (field of view = 24 cm, TR = 57 ms, TE1/ΔTE = 4.3/4.8 ms, number of TEs = 11, acquisition matrix = 416 × 320, readout bandwidth = 244 Hz/pixel, slice thickness = 3 mm, flip angle = 20°). Patient details are listed in Table 1.

2.2. Image processing

Using multi-echo GRE images, conventional MEDI and MEDI + 0 were performed to generate distinct quantitative susceptibility maps for each case. The MEDI + 0 processing method was recently described [41]: briefly, ventricular CSF is automatically segmented by thresholding the R_2^* map ($R_2^* < 5\,s^{-1}$) and applying voxel connectivity. Then, ventricular CSF uniformity is imposed in the QSM reconstruction through an additional cost energy of the CSF susceptibility variation. Lastly, a susceptibility value for the average ventricular CSF is set to zero.

2.3. Qualitative image analysis

Two experienced neuroradiologists (7 and 22 years of experience) independently assessed QSM images of both MEDI + 0 and MEDI. First, they used a three-point scale to score MEDI + 0 image quality in the 393 consecutive cases: 3, excellent (no obvious artifacts); 2, diagnostic; 1, poor. Then, they scored image concordance between MEDI + 0 and MEDI in the 393 consecutive cases using a five-point scale: 5, excellent concordance (no detectable difference); 4, good concordance (approximately 0–5% of the image contained a region with moderate difference in any axial section); 3, intermediate concordance (approximately 5–15% of the image contained a region with moderate difference in any axial section); 2, poor concordance (approximately 15–30% of the image had a moderate difference in any axial section); 1, no concordance (otherwise). The automatically generated CSF mask in MEDI + 0 was also reviewed by neuroradiologists to evaluate if they located entirely within the ventricular CSF. Representative examples are shown in Fig. 1.

2.4. Quantitative image analysis comparing the susceptibility between MEDI + 0 and MEDI

For the 20 brain glioma, 21 ischemic stroke and 43 MS cases, lesions were all segmented by an experienced neuroradiologist (7 years). Cysts and necrotic tissue were excluded from the glioma lesion segmentation. The contralateral normal appearing white matter (NAWM) were also segmented by drawing an ROI in the contralateral WM area that had a similar volume while also avoiding any lesions [10,12,42]. Lesion susceptibility values that were referenced to contralateral NAWM calculated with both MEDI + 0 and MEDI were compared.

To compute the ventricular CSF susceptibility variations in the 393 consecutive cases, the susceptibility of ventricular CSF was measured using the automatically generated CSF mask for both MEDI and MEDI + 0. MS patients from this cohort were selected for quantitative lesion

Table 1
Patient characteristics and demographics.

	Disease category	No. (scaner1/scaner2/scaner3)	Gender (M/F)	Age (years, mean ± SD)
Consecutive data from one month (393)	Cerebral vascular diseases	57 (17/16/24)	20/37	58.2 ± 19.4
	Brain tumor	107 (35/17/55)	48/59	51.7 ± 20.7
	Demyelinating diseases (e.g., MS)	37 (0/1/36)	19/18	46.1 ± 13.1
	Neurodegenerative diseases	10 (2/0/8)	6/4	74.7 ± 12.6
	Psychiatric diseases	9 (7/2/0)	4/5	45.8 ± 20.8
	Intracranial hemorrhage	16 (4/5/7)	9/7	57.3 ± 15.7
	Traumatic brain injury	5 (0/3/2)	4/1	34.0 ± 24.1
	Intracranial infection	7 (1/3/3)	4/3	43.6 ± 28.1
	Metabolic/hereditary diseases	6 (2/2/2)	5/1	27.7 ± 29.8
	Seizure	16 (7/4/5)	4/12	26.0 ± 21.2
	Newborn	6 (3/3/0)	2/4	0.1 ± 0.2
	Motor neuron diseases	5 (1/1/3)	2/3	39.0 ± 22.9
	Chiari malformation	6 (2/0/4)	1/5	24.7 ± 18.8
	Intracranial benign cyst	3 (1/1/1)	1/2	9.8 ± 16.6
	Nonspecific neurologic complaints (e.g., dizziness/headache)	103 (18/35/50)	37/66	53.2 ± 22.1
Lesion-segmented dataset (84)	Brain glioma	20 (0/20/0)	13/7	46.6 ± 12.3
	Ischemic stroke	21 (0/21/0)	16/5	52.3 ± 9.9
	Multiple sclerosis	43 (0/0/43)	14/29	43.6 ± 10.7

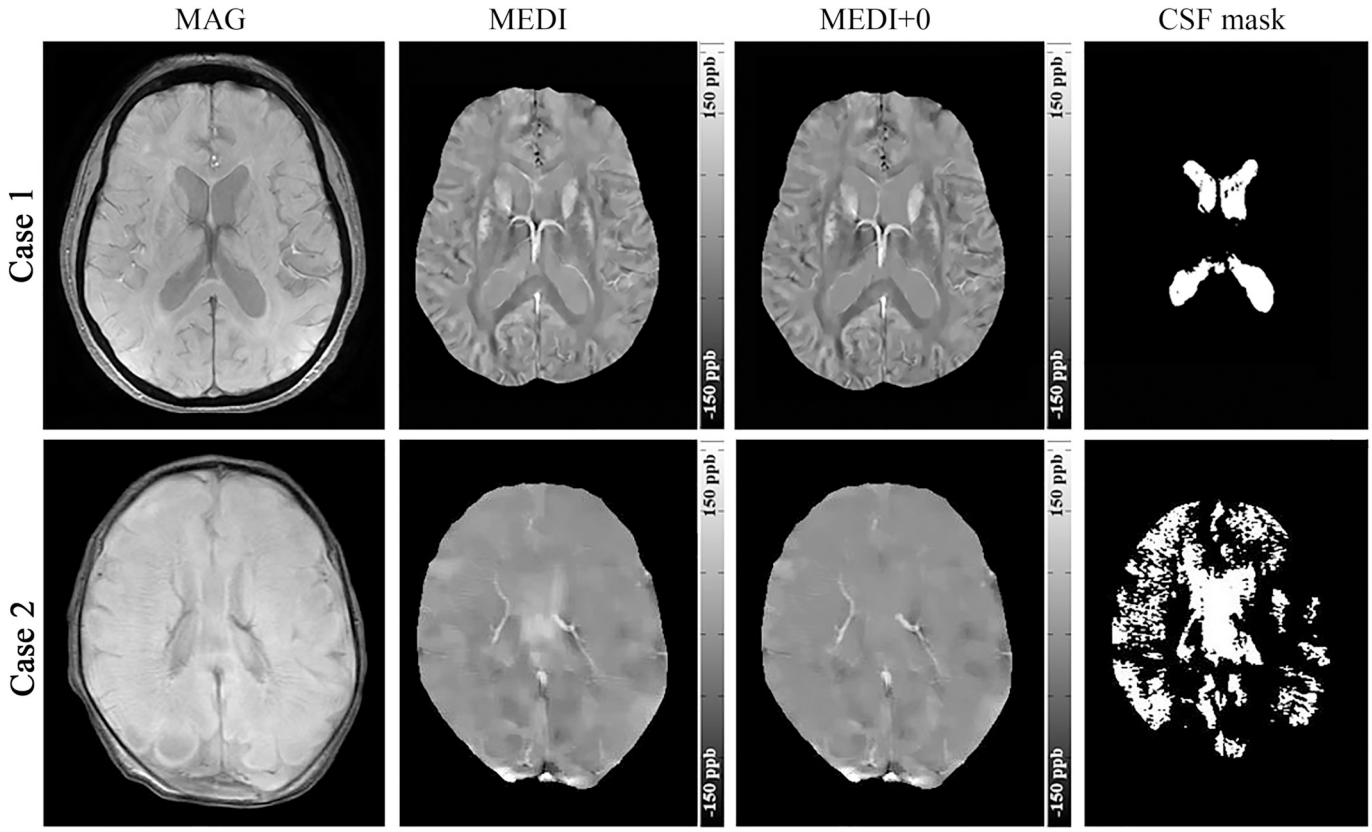

Fig. 1. The magnitude image of the gradient echo sequence (MAG), two QSM images (MEDI and MEDI + 0), and CSF mask used for zero reference in MEDI + 0 reconstruction, for two representative cases. Case 1 (top row), 79-year-old female with dizziness for 2 days showing excellent concordance between MEDI and MEDI + 0. The CSF mask was located in the ventricular CSF. Case 2 (bottom row), 5-day-old male infant with intermediate concordance. There were errors in CSF mask computation; mask extended to the white matter that contains more water in infants.

analysis. MS lesions were identified using the standard clinical imaging sequences. Lesion age was estimated by comparing with previous MRI exams, and defined as the time between its first appearance and current MRI. The MS lesion enhancing status was recorded on corresponding T1w + Gd images. Susceptibility values were averaged on MS lesion ROIs, traced on FLAIR by an experienced neuroradiologist (7 years), and measured using CSF as a zero reference. Finally, the susceptibility time course of MS lesions [12,14], which has been found to be useful for eliminating Gd injection in monitoring MS patients [11,42], was plotted.

2.5. Statistical analysis

The weighted kappa index (weight type: linear) was calculated to assess the agreement between the two neuroradiologists' evaluations. Weights were assigned to the frequencies in the nondiagonal cells of the contingency table according to their distance from the diagonal, with the magnitude of the weight diminishing the further the cell was from the diagonal [43]. Image quality of MEDI + 0 and MEDI between neuroradiologists and image concordance between MEDI + 0 and MEDI were evaluated to determine the performance of MEDI + 0 in clinical practice. The Kruskal-Wallis test was performed to compare the patient population and image quality among scanners. A Pearson correlation and Bland-Altman analysis were performed to evaluate lesion susceptibility agreement between MEDI + 0 and MEDI in glioma, ischemic stroke, and multiple sclerosis cases. All statistical analyses were performed with SPSS for Windows (version 22.0, Chicago, IL). $p < 0.05$ was recognized as statistically significant.

3. Results

3.1. Qualitative analysis comparing MEDI + 0 with MEDI

The 393 consecutive cases consisted of patients with a range of known or suspected neurological disorders (Table 1). The image quality of MEDI + 0 was scored by the two neuroradiologists as excellent in 351 (89.3%) and 362 (92.1%) cases, diagnostic in 29 (7.4%) and 24 (6.1%) cases, and poor in 13 (3.3%) and 7 (1.8%) cases (Table 2), respectively. MEDI images received similar image scores (Table 2). There were substantial agreements between the two neuroradiologists' evaluations on the image quality of MEDI + 0 (weighted kappa = 0.71; 95% CI, 0.60–0.82; percentage of agreement, 93.6% (368 of 393)) and MEDI (weighted kappa = 0.72; 95% CI, 0.61–0.82; percentage of agreement, 93.4% (367 of 393)). Among the three scanners, there was a difference in the patient distribution among disease categories ($p = 0.036$, Table 1), and there was a difference in the image quality of MEDI + 0

Table 2
Image quality (3, excellent; 2, diagnostic; 1, poor) of MEDI + 0 and MEDI of 393 cases assessed by two neuroradiologists.

		Neuroradiologist2							
		MEDI + 0				MEDI			
		3	2	1	Total	3	2	1	Total
Neuroradiologist1	3	347	4	–	351	343	7	–	350
	2	15	14	–	29	13	17	–	30
	1	–	6	7	13	–	6	7	13
Total		362	24	7	393	356	30	7	393

Table 3
Distribution among three scanners of image quality (3, excellent; 2, diagnostic; 1, poor) of MEDI + 0 and MEDI of 393 cases assessed by two neuroradiologists.

		MEDI + 0 quality				MEDI quality			
		3	2	1	Total	3	2	1	Total
Neuroradiologist1	Scanner1	92	5	3	100	92	5	3	100
	Scanner2	78	11	4	93	75	14	4	93
	Scanner3	192	8	0	200	189	11	0	200
Total		362	24	7	393	356	30	7	393
Neuroradiologist2	Scanner1	90	5	5	100	90	5	5	100
	Scanner2	74	12	7	93	74	12	7	93
	Scanner3	187	12	1	200	186	13	1	200
Total		351	29	13	393	350	30	13	393

Table 4
Comparative assessment of image concordance (5 to 1) between two neuroradiologists' evaluations.

		Neuroradiologist2					Total
		5	4	3	2	1	
Neuroradiologist1	5	345	19	–	–	–	364
	4	5	5	3	–	–	13
	3	1	7	6	–	–	14
	2	–	–	–	2	–	2
	1	–	–	–	–	–	0
Total		351	31	9	2	0	393

Data are given as n. 5, excellent concordance; 4, good concordance; 3, intermediate concordance; 2, poor concordance; 1, no concordance.

(neuroradiologist 1: $p = 0.001$; neuroradiologist 2: $p = 0.001$), and MEDI (neuroradiologist 1: $p = 0.001$; neuroradiologist 2: $p = 0.002$) (Table 3).

The concordance between MEDI + 0 and MEDI was scored by two neuroradiologists as excellent in 364 (92.6%) and 351 (89.3%) cases (Fig. 2), good in 13 (3.3%) and 31 (7.9%) cases, intermediate in 14 (3.6%) and 9 (2.3%) cases, poor in 2 (0.5%) and 2 (0.5%) cases, and none in 0 (0%) and 0 (0%) cases (Table 4), respectively. There were substantial agreements between the two neuroradiologists' evaluations on the image concordance between MEDI + 0 and MEDI (weighted kappa = 0.62; 95% CI, 0.50–0.74; percentage of agreement, 91.1% (358 of 393).

The automated R_2* based segmentation in MEDI + 0 captured the ventricles in all of the consecutive 393 (100%) cases with extension beyond the ventricles in 29 cases (7.4%, 3 cases of brain cyst, 6 cases with severe edema, 6 cases of newborn brains, 1 case of vascular malformations, 1 case of hemorrhage, 2 cases with enlarged subarachnoid space, 4 cases of other nonspecific diseases, and 6 cases with movement and metal artifacts) and to capture the ventricles only in the 20 brain glioma, 21 ischemic stroke and 43 MS cases with lesion segmentations.

3.2. Quantitatively comparing susceptibility measurements between MEDI + 0 and MEDI

As shown in Fig. 3, there was good correlation in lesion susceptibility measurements between MEDI + 0 and MEDI for glioma ($R = 0.988$, $p < 0.001$), ischemic stroke ($R = 0.978$, $p < 0.001$), and MS ($R = 0.978$, $p < 0.001$). Bland-Altman plots showed good agreements for glioma (bias 0.56 ppb, 95% limits of agreement [−5.81, 6.92] ppb), ischemic stroke (bias 0.67 ppb, 95% limits of agreement [−6.50, 5.17] ppb), and MS (bias 0.24 ppb, 95% limits of agreement [−6.34, 5.86] ppb).

For all 393 consecutive cases, variations in ventricular CSF susceptibility were reduced from MEDI (range [−28.643, 30.355] ppb, mean ± standard deviation 6.253 ± 9.352 ppb) to MEDI + 0 (range [−6.873, 10.742], −0.012 ± 1.035 ppb, $p < 0.001$). From this cohort, 67 MS lesions (including 8 acute enhancing lesions) from 27

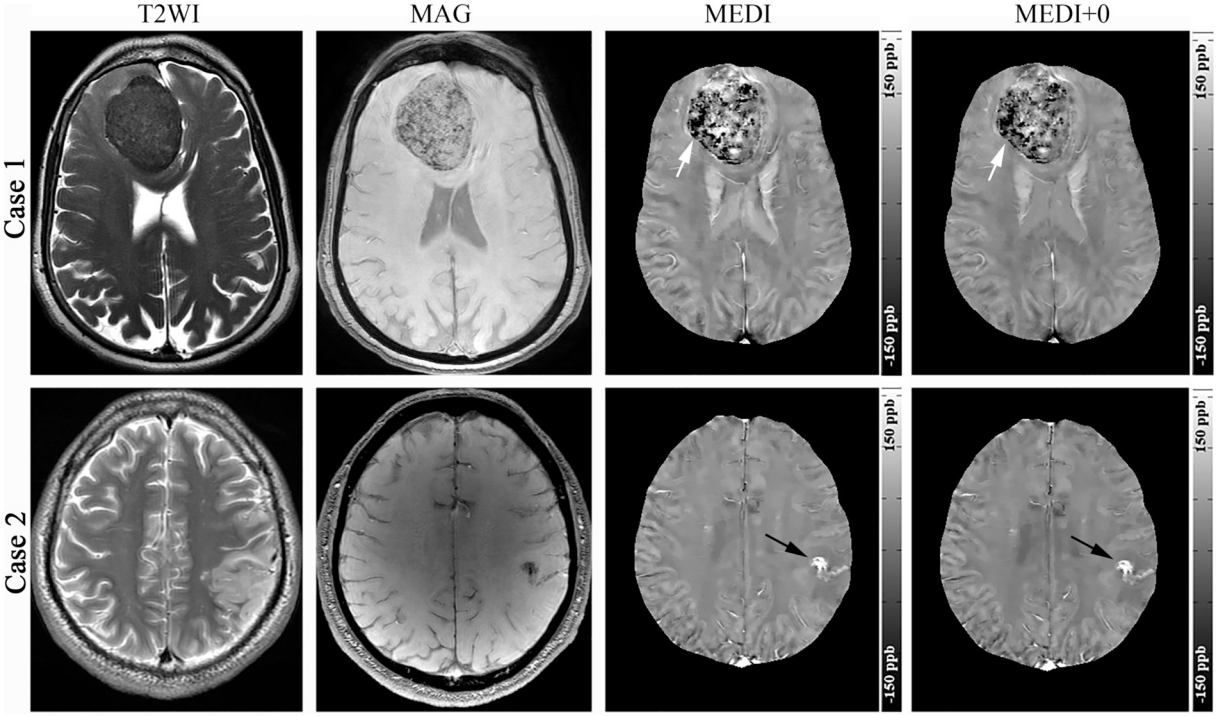

Fig. 2. Two representative cases of meningioma and ischemic stroke. Case 1 (top row), a 65-year-old female with a right frontal meningioma along the anterior falx. Diffuse calcification with diamagnetic properties can be seen within the tumor (hypointense area on QSM images, white arrow). Case 2 (bottom row), a 51-day-old male ischemic stroke patient with hemorrhage transformation in the left parietal lobe (hyperintense area on QSM images, black arrow). Both cases showed excellent concordance between MEDI and MEDI + 0.

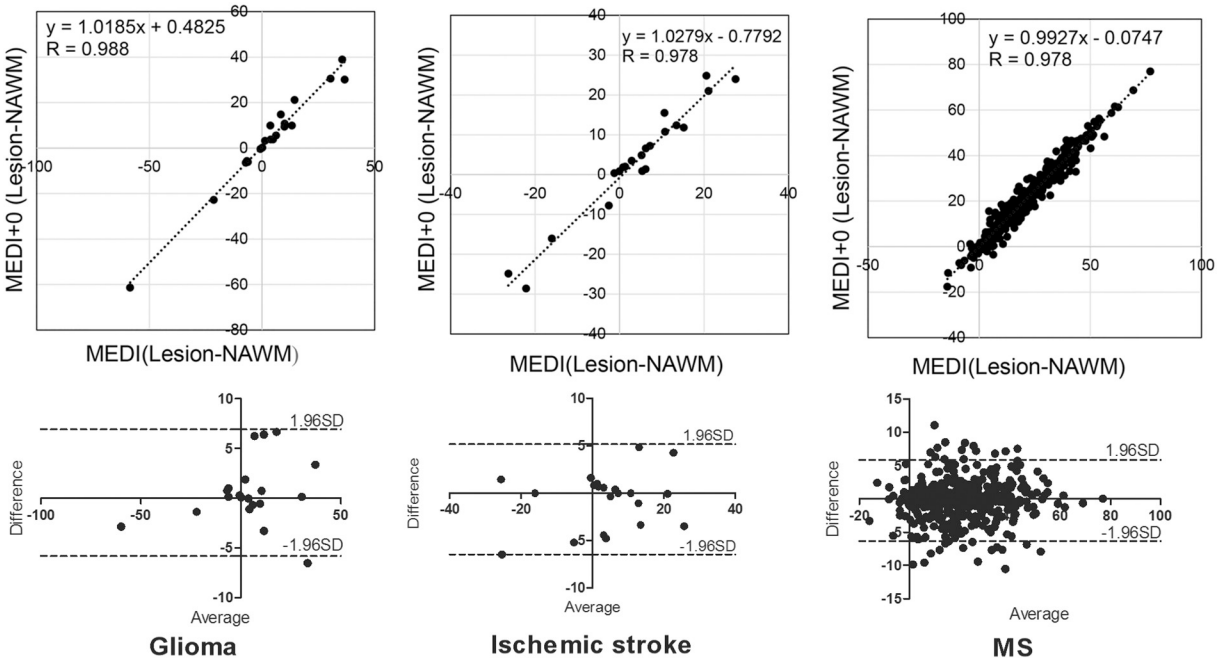

Fig. 3. Linear regression and Bland-Altman plots for lesion susceptibility values (in ppb) between MEDI + 0 and MEDI in glioma (left), ischemic stroke (mid) and MS (right). Lesion susceptibility values relative to NAWM measured by MEDI + 0 and MEDI agreed well with each other.

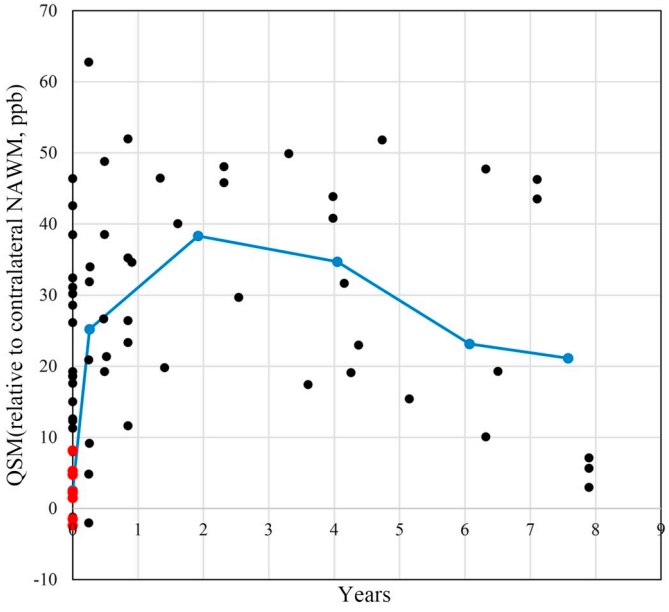

Fig. 4. The time course of MS lesion susceptibility relative to contralateral NAWM (using MEDI + 0). The susceptibility of MS lesions showed increase in the first 2 years, then started to decrease slowly. The red dots represent acute enhancing MS lesions, the black dots represent chronic nonenhancing MS lesions, and the blue line represents the average susceptibility in the enhancing, and nonenhancing 0–1, 1–3, 3–5, 5–7, 7–9 year age groups. (For interpretation of the references to colour in this figure legend, the reader is referred to the web version of this article.)

patients had identifiable first-appearance in patient MRI record. The time course of lesion susceptibility relative to contralateral NAWM (using MEDI + 0) is shown in Fig. 4. The susceptibility of MS lesions showed an initial jump from enhancing to non-enhancing, then an increasing trend in the first 2 years, followed by a decreasing trend thereafter. Fig. 5 shows examples of one MS lesion that is hyperintense on QSM and nonenhancing on T1w + Gd, and another lesion that is isointense on QSM but enhancing on T1w + Gd.

4. Discussion

Our results show that brain QSM can be automatically generated with reliable image quality for clinical purposes in a wide range of pathophysiological conditions, including glioma, ischemic stroke, and multiple sclerosis. QSM generated from MEDI + 0 is in excellent or good concordance with QSM from MEDI. MEDI + 0 with automatic CSF zero reference provides susceptibility values that may be very useful for longitudinal and cross-center studies.

As judged by two experienced neuroradiologists, QSM generated by MEDI + 0 in clinical MRI has very reliable image quality. To produce a broad image quality assessment with minimal selection bias, image analyses were performed on all consecutive cases from 3 scanners in a single month at our institution. MEDI + 0 automatically referenced to CSF provided excellent image quality in an average of 90.7% cases, and excellent or diagnostic quality in an average of 97.5% cases. The poor image quality in the remaining 2.5% cases was caused by motion or metallic artifacts in the original gradient echo data prior to QSM postprocessing. Though we did not check the image quality of other sequences in the clinical MRI, the success rate of QSM performance in clinical practice is consistent with the success rate of standard sequences in clinical MRI. QSM has been demonstrated to be highly reproducible on a single scanner [44–47] and among multiple vendors, sites, and field strengths [45,48–52]. The observed difference in image quality among scanners at our institution (Table 3) may be attributed to the difference in patient population (Table 1). Patient severity for the outpatient facility scanner 3 with the highest image quality is less than that for inpatient facility scanners 1 and 2. It is known that patient severity degrades MRI quality, possibly caused by motion and implant artifacts [51].

Lesion susceptibility contrast did not change due to zero reference, as expected and demonstrated quantitatively in cases of brain glioma, ischemic stroke, and MS. The lesion to NAWM contrast on QSM from MEDI + 0 is in good agreement with that obtained from MEDI, as demonstrated by linear regression and the Bland-Altman analysis. This implies that the lesion to NAWM contrast in multiple sclerosis MEDI

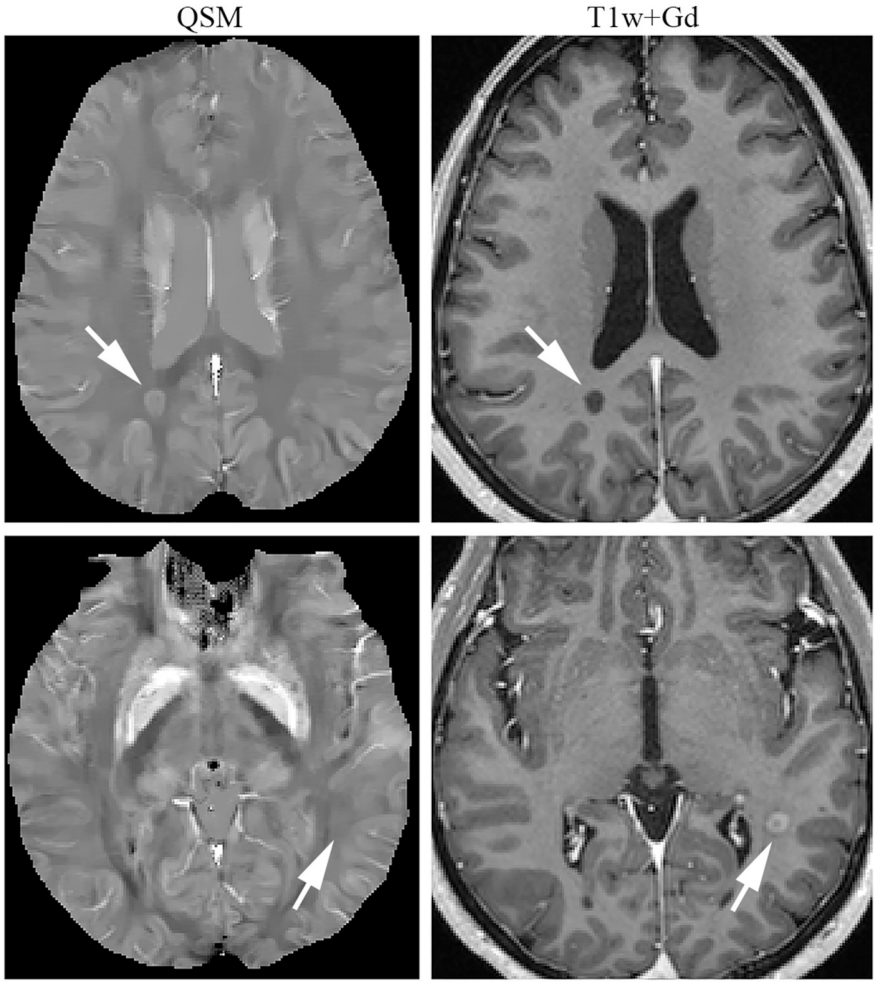

Fig. 5. One 42-year-old female MS patient with both enhancing and nonenhancing lesions. One MS lesion showed QSM hyperintense, which is predictive of nonenhancing lesions as confirmed on T1w + Gd image (top row, arrows); while the other lesion showed QSM isointense, which is predictive of enhancing lesion as confirmed on T1w + Gd images (bottom row, arrows).

studies reported in the literature [12–14,53] can still be used for direct comparison with MEDI + 0.

The time course of MS lesion susceptibility measured in this cohort of patients (Fig. 4) has a similar trend as that reported in a previous study [14]: isointense initially for acute enhancing lesions, followed by a rapid rise to hyperintensity after enhancement cessation, and then remaining hyperintense over many years for active chronic lesions. This MS lesion susceptibility time course is supported by the underlying biophysics [54,55]. The blood brain barrier seals after one month, but by this time there has already been substantial myelin digestion, exit of macrophages laden with myelin debris from the lesion center, and possible accumulation of proinflammatory microglia loaded with iron, ultimately resulting in long lasting chronic inflammation. As illustrated in Fig. 5, QSM hyperintensity is mathematically complimentary to gadolinium (Gd) enhancement, allowing for an accurate prediction of Gd enhancement status of MS lesions without the need for repeated Gd injections during MS patient monitoring [11,42].

MEDI + 0 represents a very useful technical advancement over MEDI because it provides susceptibility values that are automatically referenced to CSF while also improving image quality. For brain QSM, ventricular CSF devoid of cellular contents represents an ideal zero reference. The low R_2* value of CSF allows for it to be automatically segmented. The regularization of imposing a realistically homogeneous susceptibility value on CSF (MEDI + 0) helps project out shadow artifacts caused by anisotropic white matter surrounding the CSF [41,56]. Without this CSF zero regularization, CSF is contaminated by inhomogeneous susceptibility in conventional QSM, making it a suboptimal reference. More importantly, MEDI + 0 enables that tissue susceptibility values can be used directly in longitudinal and cross-center studies, particularly those with voxel/atlas based analyses [15,57,58].

The automated CSF mask in MEDI + 0 was found to be located entirely within the ventricular CSF in most cases, and the majority of QSM maps reconstructed by MEDI + 0 and MEDI had excellent or good concordance. The R_2*-based segmentation in MEDI + 0 fundamentally identifies large connected regions of uniform susceptibility for use as a reference and for projecting out anisotropy artifacts [41], and the ventricular CSF with minimal cellular contents renders it a natural target for segmentation. Edema may cause this R_2* based segmentation to extend beyond brain ventricles, but will not affect the performance of MEDI + 0. The segmentation may include brain parenchyma with abnormally high water content due to the presence of cysts, severe edema (hyperintensity on T2w can cause low R_2*), newborn brains (whose white matter contains more water), vascular malformations (malformed enlarged vessels contain more water), hemorrhage (causing severe edema), and other nonspecific diseases, as well as an enlarged subarachnoid space due to severe brain atrophy in the elderly, or patients with olivopontocerebellar atrophy (OPCA) [59,60]. Therefore, the QSM images reconstructed by MEDI + 0 depict the underlying pathologies according to their effects on water content in the brain parenchyma. Conversely, the R_2*-based CSF segmentation would exclude high-R_2* structures in ventricles, include the choroid plexus (vessels and

calcifications), hemorrhage [41], and artifacts associated with motion and implants (n = 6). Except for intraventricular hemorrhage, there are no other known major diseases that cause substantial R_2* changes in the CSF [61]; the evaluated antibody (immunoglobulin) concentration in CSF from an MS brain is still too low (< 1 ppb in weight [62]) to cause a detectable increase in R_2*. However, this MEDI + 0 approach fails to measure the subtle susceptibility within the CSF due to the automated zero reference procedure.

Despite avoiding selection bias by analyzing all scans within a single month, we could better validate QSM by expanding the time frame to include more cases, and we could expand quantitative analyses beyond brain glioma, ischemia, and multiple sclerosis lesions. It should be cautioned that MEDI + 0 and MEDI solve only the inverse problem for scalar susceptibility [31,41], which is a good approximation for biometals with strong susceptibility and for most MS lesions that are completely demyelinated [4]. The susceptibility anisotropy of white matter myelin makes its susceptibility value dependent on its orientation in the magnet [34,38–40] and therefore it is difficult to determine even with impractically using 12 orientations [35–37]. MEDI + 0 tends to reduce the white matter anisotropy effects in QSM [41], contrast to NAWM may still be used in reporting lesion susceptibility value, and scalar susceptibility may be meaningfully used for lesions dominated by scalar susceptibility source. Automated CSF segmentation may be easily extended from the multi-echo GRE acquisition using a simple R_2*-thresholding to the single-echo acquisition similar to that in susceptibility weighted imaging (SWI) using the central bright signal characteristics and various computer vision algorithms including latest artificial intelligence approach [63–65].

In conclusion, brain QSM demonstrates reliable diagnostic quality in clinical practice for studying various neurological diseases. MEDI + 0 reconstruction with automated CSF zero reference regularization does not change lesion contrast. Brain QSM with MEDI + 0 can be applied in daily clinical practice, particularly for quantitative brain studies.

Funding

This work was supported in part by grants from the National Institutes of Health (R01NS090464, R01NS095562, R21EB024366, S10OD021782, R01CA181566) and the National Multiple Sclerosis Society (RG-1602-07671).

Declarations of interest

None.

References

[1] Li J, Chang S, Liu T, Wang Q, Cui D, Chen X, et al. Reducing the object orientation dependence of susceptibility effects in gradient echo MRI through quantitative susceptibility mapping. Magn Reson Med 2012;68(5):1563–9.
[2] Zhou D, Liu T, Spincemaille P, Wang Y. Background field removal by solving the Laplacian boundary value problem. NMR Biomed 2014;27(3):312–9.
[3] de Rochefort L, Liu T, Kressler B, Liu J, Spincemaille P, Lebon V, et al. Quantitative susceptibility map reconstruction from MR phase data using Bayesian regularization: validation and application to brain imaging. Magn Reson Med 2010;63(1):194–206.
[4] Wang Y, Spincemaille P, Liu Z, Dimov A, Deh K, Li J, et al. Clinical quantitative susceptibility mapping (QSM): biometal imaging and its emerging roles in patient care. J Magn Reson Imaging 2017;46(4):951–71.
[5] Wang Y, Liu T. Quantitative susceptibility mapping (QSM): decoding MRI data for a tissue magnetic biomarker. Magn Reson Med 2015;73(1):82–101.
[6] Haacke EM, Liu S, Buch S, Zheng W, Wu D, Ye Y. Quantitative susceptibility mapping: current status and future directions. Magn Reson Imaging 2015;33(1):1–25.
[7] Liu C, Li W, Tong KA, Yeom KW, Kuzminski S. Susceptibility-weighted imaging and quantitative susceptibility mapping in the brain. J Magn Reson Imaging 2015;42(1):23–41.
[8] Reichenbach JR, Schweser F, Serres B, Deistung A. Quantitative susceptibility mapping: concepts and applications. Clin Neuroradiol 2015;25(Suppl. 2):225–30.
[9] Langkammer C, Liu T, Khalil M, Enzinger C, Jehna M, Fuchs S, et al. Quantitative susceptibility mapping in multiple sclerosis. Radiology 2013;267(2):551–9.
[10] Chen W, Zhang Y, Mu K, Pan C, Gauthier SA, Zhu W, et al. Quantifying the susceptibility variation of normal-appearing white matter in multiple sclerosis by quantitative susceptibility mapping. AJR Am J Roentgenol 2017:1–6.
[11] Zhang Y, Gauthier SA, Gupta A, Tu L, Comunale J, Chiang GC, et al. Magnetic susceptibility from quantitative susceptibility mapping can differentiate new enhancing from nonenhancing multiple sclerosis lesions without gadolinium injection. AJNR Am J Neuroradiol 2016;37(10):1794–9.
[12] Zhang Y, Gauthier SA, Gupta A, Comunale J, Chia-Yi Chiang G, Zhou D, et al. Longitudinal change in magnetic susceptibility of new enhanced multiple sclerosis (MS) lesions measured on serial quantitative susceptibility mapping (QSM). J Magn Reson Imaging 2016;44(2):426–32.
[13] Zhang Y, Gauthier SA, Gupta A, Chen W, Comunale J, Chiang GC, et al. Quantitative susceptibility mapping and R2* measured changes during white matter lesion development in multiple sclerosis: myelin breakdown, myelin debris degradation and removal, and iron accumulation. AJNR Am J Neuroradiol 2016;37(9):1629–35.
[14] Chen W, Gauthier SA, Gupta A, Comunale J, Liu T, Wang S, et al. Quantitative susceptibility mapping of multiple sclerosis lesions at various ages. Radiology 2014;271(1):183–92.
[15] Cobzas D, Sun H, Walsh AJ, Lebel RM, Blevins G, Wilman AH. Subcortical gray matter segmentation and voxel-based analysis using transverse relaxation and quantitative susceptibility mapping with application to multiple sclerosis. J Magn Reson Imaging 2015;42(6):1601–10.
[16] Eskreis-Winkler S, Deh K, Gupta A, Liu T, Wisnieff C, Jin M, et al. Multiple sclerosis lesion geometry in quantitative susceptibility mapping (QSM) and phase imaging. J Magn Reson Imaging 2015;42(1):224–9.
[17] Kakeda S, Futatsuya K, Ide S, Watanabe K, Miyata M, Moriya J, et al. Improved detection of cortical gray matter involvement in multiple sclerosis with quantitative susceptibility mapping. Acad Radiol 2015;22(11):1427–32.
[18] Wisnieff C, Ramanan S, Olesik J, Gauthier S, Wang Y, Pitt D. Quantitative susceptibility mapping (QSM) of white matter multiple sclerosis lesions: interpreting positive susceptibility and the presence of iron. Magn Reson Med 2015;74(2):564–70.
[19] Barbosa JH, Santos AC, Tumas V, Liu M, Zheng W, Haacke EM, et al. Quantifying brain iron deposition in patients with Parkinson's disease using quantitative susceptibility mapping, R2 and R2. Magn Reson Imaging 2015;33(5):559–65.
[20] He N, Ling H, Ding B, Huang J, Zhang Y, Zhang Z, et al. Region-specific disturbed iron distribution in early idiopathic Parkinson's disease measured by quantitative susceptibility mapping. Hum Brain Mapp 2015;36(11):4407–20.
[21] Ide S, Kakeda S, Ueda I, Watanabe K, Murakami Y, Moriya J, et al. Internal structures of the globus pallidus in patients with Parkinson's disease: evaluation with quantitative susceptibility mapping (QSM). Eur Radiol 2015;25(3):710–8.
[22] Du G, Liu T, Lewis MM, Kong L, Wang Y, Connor J, et al. Quantitative susceptibility mapping of the midbrain in Parkinson's disease. Mov Disord 2016;31(3):317–24.
[23] Ciraci S, Gumus K, Doganay S, Dundar MS, Kaya Ozcora GD, Gorkem SB, et al. Diagnosis of intracranial calcification and hemorrhage in pediatric patients: comparison of quantitative susceptibility mapping and phase images of susceptibility-weighted imaging. Diagn Interv Imaging 2017;98(10):707–14.
[24] Zeineddine HA, Girard R, Cao Y, Hobson N, Fam MD, Stadnik A, et al. Quantitative susceptibility mapping as a monitoring biomarker in cerebral cavernous malformations with recent hemorrhage. J Magn Reson Imaging 2018;47(4):1133–8.
[25] Chen W, Zhu W, Kovanlikaya I, Kovanlikaya A, Liu T, Wang S, et al. Intracranial calcifications and hemorrhages: characterization with quantitative susceptibility mapping. Radiology 2014;270(2):496–505.
[26] Sun H, Kate M, Gioia LC, Emery DJ, Butcher K, Wilman AH. Quantitative susceptibility mapping using a superposed dipole inversion method: application to intracranial hemorrhage. Magn Reson Med 2016;76(3):781–91.
[27] Liu T, Surapaneni K, Lou M, Cheng L, Spincemaille P, Wang Y. Cerebral microbleeds: burden assessment by using quantitative susceptibility mapping. Radiology 2012;262(1):269–78.
[28] Deistung A, Schweser F, Wiestler B, Abello M, Roethke M, Sahm F, et al. Quantitative susceptibility mapping differentiates between blood depositions and calcifications in patients with glioblastoma. PLoS One 2013;8(3):e57924.
[29] Liu T, Wisnieff C, Lou M, Chen W, Spincemaille P, Wang Y. Nonlinear formulation of the magnetic field to source relationship for robust quantitative susceptibility mapping. Magn Reson Med 2013;69(2):467–76.
[30] Liu T, Xu W, Spincemaille P, Avestimehr AS, Wang Y. Accuracy of the morphology enabled dipole inversion (MEDI) algorithm for quantitative susceptibility mapping in MRI. IEEE Trans Med Imaging 2012;31(3):816–24.
[31] Liu J, Liu T, de Rochefort L, Ledoux J, Khalidov I, Chen W, et al. Morphology enabled dipole inversion for quantitative susceptibility mapping using structural consistency between the magnitude image and the susceptibility map. Neuroimage 2012;59(3):2560–8.
[32] Straub S, Schneider TM, Emmerich J, Freitag MT, Ziener CH, Schlemmer HP, et al. Suitable reference tissues for quantitative susceptibility mapping of the brain. Magn Reson Med 2017;78(1):204–14.
[33] Duyn JH, van Gelderen P, Li TQ, de Zwart JA, Koretsky AP, Fukunaga M. High-field MRI of brain cortical substructure based on signal phase. Proc Natl Acad Sci U S A 2007;104(28):11796–801.
[34] Lee J, Shmueli K, Fukunaga M, van Gelderen P, Merkle H, Silva AC, et al. Sensitivity of MRI resonance frequency to the orientation of brain tissue microstructure. Proc Natl Acad Sci U S A 2010;107(11):5130–5.
[35] Li X, Vikram DS, Lim IA, Jones CK, Farrell JA, van Zijl PC. Mapping magnetic susceptibility anisotropies of white matter in vivo in the human brain at 7 T. Neuroimage 2012;62(1):314–30.
[36] Wisnieff C, Liu T, Spincemaille P, Wang S, Zhou D, Wang Y. Magnetic susceptibility anisotropy: cylindrical symmetry from macroscopically ordered anisotropic

molecules and accuracy of MRI measurements using few orientations. Neuroimage 2013;70:363–76.
[37] Liu C. Susceptibility tensor imaging. Magn Reson Med 2010;63(6):1471–7.
[38] Yablonskiy DA, Luo J, Sukstanskii AL, Iyer A, Cross AH. Biophysical mechanisms of MRI signal frequency contrast in multiple sclerosis. Proc Natl Acad Sci U S A 2012;109(35):14212–7.
[39] Yablonskiy DA, Sukstanskii AL. Generalized Lorentzian Tensor Approach (GLTA) as a biophysical background for quantitative susceptibility mapping. Magn Reson Med 2015;73(2):757–64.
[40] Wharton S, Bowtell R. Effects of white matter microstructure on phase and susceptibility maps. Magn Reson Med 2015;73(3):1258–69.
[41] Liu Z, Spincemaille P, Yao Y, Zhang Y, Wang Y. MEDI + 0: morphology enabled dipole inversion with automatic uniform cerebrospinal fluid zero reference for quantitative susceptibility mapping. Magn Reson Med 2018;79(5):2795–803.
[42] Zhang S, Nguyen TD, Zhao Y, Gauthier SA, Wang Y, Gupta A. Diagnostic accuracy of semiautomatic lesion detection plus quantitative susceptibility mapping in the identification of new and enhancing multiple sclerosis lesions. Neuroimage Clin 2018;18:143–8.
[43] Watson PF, Petrie A. Method agreement analysis: a review of correct methodology. Theriogenology 2010;73(9):1167–79.
[44] Deh K, Nguyen TD, Eskreis-Winkler S, Prince MR, Spincemaille P, Gauthier S, et al. Reproducibility of quantitative susceptibility mapping in the brain at two field strengths from two vendors. J Magn Reson Imaging 2015;42(6):1592–600.
[45] Hinoda T, Fushimi Y, Okada T, Fujimoto K, Liu C, Yamamoto A, et al. Quantitative susceptibility mapping at 3 T and 1.5 T: evaluation of consistency and reproducibility. Invest Radiol 2015;50(8):522–30.
[46] Lin PY, Chao TC, Wu ML. Quantitative susceptibility mapping of human brain at 3T: a multisite reproducibility study. AJNR Am J Neuroradiol 2015;36(3):467–74.
[47] Santin MD, Didier M, Valabregue R, Yahia Cherif L, Garcia-Lorenzo D, Loureiro de Sousa P, et al. Reproducibility of R2 * and quantitative susceptibility mapping (QSM) reconstruction methods in the basal ganglia of healthy subjects. NMR Biomed 2017;30(4).
[48] Blazejewska AI, Al-Radaideh AM, Wharton S, Lim SY, Bowtell RW, Constantinescu CS, et al. Increase in the iron content of the substantia nigra and red nucleus in multiple sclerosis and clinically isolated syndrome: a 7 Tesla MRI study. J Magn Reson Imaging 2015;41(4):1065–70.
[49] Deh K, Kawaji K, Bulk M, Van Der Weerd L, Lind E, Spincemaille P, et al. Multicenter reproducibility of quantitative susceptibility mapping in a gadolinium phantom using MEDI + 0 automatic zero referencing. Magn Reson Med 2019;81(2):1229–36.
[50] Jafari R, Sheth S, Spincemaille P, Nguyen TD, Prince MR, Wen Y, et al. Rapid automated liver quantitative susceptibility mapping. J Magn Reson Imaging 2019. https://doi.org/10.1002/jmri.26632.
[51] Andre JB, Bresnahan BW, Mossa-Basha M, Hoff MN, Smith CP, Anzai Y, et al. Toward quantifying the prevalence, severity, and cost associated with patient motion during clinical MR examinations. J Am Coll Radiol 2015;12(7):689–95.
[52] Wang R, Xie G, Zhai M, Zhang Z, Wu B, Zheng D, et al. Stability of R2* and quantitative susceptibility mapping of the brain tissue in a large scale multi-center study. Sci Rep 2017;7:45261.
[53] Yao Y, Nguyen TD, Pandya S, Zhang Y, Hurtado Rua S, Kovanlikaya I, et al. Combining quantitative susceptibility mapping with automatic zero reference (QSM0) and myelin water fraction imaging to quantify iron-related myelin damage in chronic active MS lesions. AJNR Am J Neuroradiol 2018;39(2):303–10.
[54] Deh K, Ponath GD, Molvi Z, Parel GT, Gillen KM, Zhang S, et al. Magnetic susceptibility increases as diamagnetic molecules breakdown: myelin digestion during multiple sclerosis lesion formation contributes to increase on QSM. J Magn Reson Imaging 2018;48(5):1281–7.
[55] Kutzelnigg A, Lassmann H. Pathology of multiple sclerosis and related inflammatory demyelinating diseases. Handb Clin Neurol 2014;122:15–58.
[56] Kee Y, Liu Z, Zhou L, Dimov A, Cho J, de Rochefort L, et al. Quantitative susceptibility mapping (QSM) algorithms: mathematical rationale and computational implementations. IEEE Trans Biomed Eng 2017;64(11):2531–45.
[57] Hanspach J, Dwyer MG, Bergsland NP, Feng X, Hagemeier J, Bertolino N, et al. Methods for the computation of templates from quantitative magnetic susceptibility maps (QSM): toward improved atlas- and voxel-based analyses (VBA). J Magn Reson Imaging 2017;46(5):1474–84.
[58] Kim HG, Park S, Rhee HY, Lee KM, Ryu CW, Rhee SJ, et al. Quantitative susceptibility mapping to evaluate the early stage of Alzheimer's disease. Neuroimage Clin 2017;16:429–38.
[59] Berciano J, Boesch S, Perez-Ramos JM, Wenning GK. Olivopontocerebellar atrophy: toward a better nosological definition. Mov Disord 2006;21(10):1607–13.
[60] Hamaguchi H, Kanda F, Hosaka K, Fujii M, Chihara K. Comparison between MRI and 3D-SSP in olivopontocerebellar atrophy and cortical cerebellar atrophy. Rinsho Shinkeigaku 2004;44(4–5):263–7.
[61] Rosenberg GA. Chapter 4 - cerebrospinal fluid: formation, absorption, markers, and relationship to blood–brain barrier. In: Caplan LR, Biller J, Leary MC, Lo EH, Thomas AJ, Yenari M, editors. Primer on cerebrovascular diseases. 2nd ed.San Diego: Academic Press; 2017. p. 25–31.
[62] Harris VK, Tuddenham JF, Sadiq SA. Biomarkers of multiple sclerosis: current findings. Degener Neurol Neuromuscul Dis 2017;7:19–29.
[63] Schnack HG, Hulshoff Pol HE, Baare WF, Viergever MA, Kahn RS. Automatic segmentation of the ventricular system from MR images of the human brain. Neuroimage 2001;14(1 Pt 1):95–104.
[64] Yepes-Calderon F, Nelson MD, McComb JG. Automatically measuring brain ventricular volume within PACS using artificial intelligence. PLoS One 2018;13(3):e0193152.
[65] Ghafoorian M, Teuwen J, Manniesing R, F-Ed Leeuw, Bv Ginneken, Karssemeijer N, et al. Student beats the teacher: deep neural networks for lateral ventricles segmentation in brain MR. SPIE 2018;10574:105742U.